Atmos. Meas. Tech. Discuss., 6, 8235–8267, 2013
www.atmos-meas-tech-discuss.net/6/8235/2013/
doi:10.5194/amtd-6-8235-2013

Atmospheric Measurement Techniques Discussions

Long-path averaged mixing ratios of O_3 and NO_2 in the free troposphere from mountain MAX-DOAS

L. Gomez[1], M. Navarro-Comas[1], O. Puentedura[1], Y. Gonzalez[2], E. Cuevas[2], and M. Gil-Ojeda[1]

[1]Instituto Nacional de Técnica Aeroespacial (INTA), Área de Investigación e Instrumentación Atmosférica, Ctra Ajalvir km4, 28850, Torrejón de Ardoz, Madrid, Spain
[2]Centro de Investigación Atmosférica de Izaña (Agencia Estatal de Meteorología – AEMET), Santa Cruz de Tenerife, Spain

Received: 7 May 2013 – Accepted: 20 August 2013 – Published: 5 September 2013

Correspondence to: L. Gomez (gomezml@inta.es)

Published by Copernicus Publications on behalf of the European Geosciences Union.

Abstract

A new approximation is proposed to estimate O_3 and NO_2 mixing ratios in the Northern Subtropics Free Troposphere (FT). Multi Axis Differential Optical Absorption Spectroscopy (MAX-DOAS) high mountain measurements, recorded at Izaña Observatory (28°18′ N, 16°29′ W), are used in this work. Proposed method uses horizontal and near-zenith geometries to estimate the station level differential path. Two different methods are described. First one uses retrieved Slant Column Densities (SCD) of O_4. On second method, path is estimated from LIBRADTRAN radiative transfer model for the region and season. Results show that under low aerosol loading, O_3 and NO_2 mixing ratios concentrations can be retrieved with moderately low errors. Obtained concentrations have been compared with in situ instrumentation on the observatory. O_3 concentration in FT is found to be in the range of 40–80 ppb, approximately. NO_2 is in the range of 20–30 ppt, below the detection limit of in situ instrumentation. The different air masses scanned by each instrument have been identified as a cause of discrepancy between O_3 observed by MAX-DOAS and in situ.

1 Introduction

Distribution of minor species in the Free Troposfere (FT) allows determining the reference background conditions for pollution studies (Engardt et al., 2009; Beelen et al., 2009). Furthermore it is also of particular interest when studying chemical processes that take place during long-range transport (Thakur et al., 1999). Pollutants can be transported over long distances through the FT, where fast winds exist and lifetime of minor species is larger (Stohl and Trickl, 1999; Stohl et al., 2003; Liang et al., 2004). Mechanisms involved require the pollutants uplifting over the Boundary Layer (BL) when meteorological conditions are favourable (Takur et al., 1999; Kolb et al., 2009). In recent years, extensive measurement programmes (Martin et al., 2009; Roscoe et al., 2010; Wagner et al., 2010) greatly improved our knowledge of global

AMTD
6, 8235–8267, 2013

distribution of minor species such as O_3 or NO_2 near the surface. Unfortunately, little is know so far concerning both the quantity of pollutant reaching the FT (Wenig et al., 2003), and the downward exchange between the FT and the lower troposphere (Zyryanov et al., 2012). Nevertheless, a better understanding of these processes can be obtained from measurements recorded in FT mountain observatories.

In FT stations, minor species measurements have traditionally been carried out by airborne devices such as chromatographs, Electro Chemical Cell (ECC) or UV absorption cell (Robinson et al., 2005; Mao et al., 2006; Hintsa et al., 2004; Martin et al., 2006; Oltmans et al., 1996; Thompson et al., 2011). Despite the high accuracy of such measurements they are seldomly performed due to their high cost. A continuous monitoring of background levels of chemically active trace gases in the FT is then limited to in situ instruments located in the few existing mountain observatories. However, measurements provided by these instruments are local and usually affected by the so called "mountain breeze effect" (MBE) (e.g. Cuevas et al., 1992; Reidmiller et al., 2012). Therefore these measurements are not representative of background conditions. The MAX-DOAS technique solves all of the above mentioned issues. On one hand, unlike the in situ measurements, MAX-DOAS integrate optical paths over few tens of km. Therefore it averages inhomogeneities in the path, which in turn minimizes the impact of the up-welling of air masses from the BL (MBE). On the other hand, MAX-DOAS allows continuous measuring as long as there is day light.

MAX-DOAS technique allows obtaining the so called Slant Column Density (SCD), which is the density of a given gas along the optical path. In order to remove the observation angle dependence on the data, SCD can be converted to the Vertical Column Density (VDC) using the Air Mass Factor (AMF). AMF, which can be calculated from Radiative Transfer Models (RTM), is closely related with the effective optical path of the measurement. The latter, needed to obtain the density at a given altitude, can be calculated using different approaches. The simplest one was introduced by Honninger (Honninger and Platt, 2002; Honninger et al., 2004). This approach only considers single scattering and does not take into account surface albedo or aerosols extinction. A more

AMTD
6, 8235–8267, 2013

realistic method that takes into account these factors consists in using RTMs together with Optimal Estimation Method (OEM) (Rodgers, 2000). OEM needs to assume an a priori profile and its corresponding covariance matrix (Rodgers, 2000). Constrains of the concentrations obtained with this method are expressed by the a priori covariance matrix. Steck (2002), introduced a modification of OEM where constrains are given by a regularization matrix. Both methods are similar and are computationally very costly. To solve this, Sinreich et al. (2012) presented a new method to obtain concentrations of trace gases in the BL when high aerosol loads are present. It considers a uniform BL where the light paths for the lowest elevation angles do not differ significantly. The optical path is then obtained from the differential SCD (DSCD) of O_4 between the observations at low Instrumental Elevation Angle (IEA) and the zenith observations. Nevertheless, when using this method, one must pay attention to situations of very high load of aerosols. In this case, scattering towards the detector happens close to it and optical paths of low and high IEA are similar, which leads to a poor performance of the model. In order to test this method, the authors used it to estimate NO_2 concentrations in the Mexico City, where high NO_2 volume mixing ratios are observed. These results are in good agreement with those obtained with another similar technique (Long Path DOAS).

Here we propose a modified version of MAX-DOAS geometric approximation (Honninger et al., 2004) to estimate FT tracers at very low concentrations. This new method, that we have called Modified Geometrical Approach (MGA), makes use of the horizontal path to obtain gases mixing ratios. Here, we consider this parameter to be the difference between the optical paths of the zenith and horizon views, and is calculated using two procedures. The first one, called O_4-MGA, makes use of the O_2 dimer measurements at the level of the station. The second one, named AMF-MGA, uses RT libradtran model to obtain the required paths. Moreover, we apply our method (MGA) to estimate the O_3 and NO_2 concentrations at Izaña Observatory. The obtained results are then compared with in situ measurement of both species. Since in situ measurements are based in different techniques/principles than DOAS (UV absorption cell for

AMTD
6, 8235–8267, 2013

O_3 and chemiluminiscence for NO_2), they are an independent and excellent set of measurement to validate the consistency of our method (MGA). MGA can also be extended to other species with structured absorption spectra in the near UV and visible ranges, such as H_2O, HCHO, CHOCHO, IO.

In Sect. 2 the station and meteorology of the area is presented. In Sect. 3 the MGA is described, and Sects. 4 and 5 deal with the different instrumentation and data. Results and discussion are provided in Sect. 6. Finally, the main conclusions are summarized in Sect. 7.

1.1 Izaña station

Izaña Atmospheric Observatory (28°18′ N, 16°29′ W) is located in Tenerife (Canary Islands), at an altitude of 2373 m a.s.l. This observatory is part of the Global Atmospheric Watch (GAW) programme and is managed by the Centro de Investigación Atmosférica de Izaña (CIAI) that belongs to the Agencia Estatal de Meteorología (AEMET, Spain). In Canary Islands, the influence of the descending branch of the Hadley Cell creates a high stability regime that results in a large number of days with clear sky and a quasi-permanent strong temperature inversion ranging between 800 and 1500 m a.s.l. (Font, 1956; Milford et al., 2008). The temperature inversion defines an upper limit to the marine boundary layer (MBL), thus it prevents pollution from lower levels to reach the FT. Therefore the Izaña station is located above the MBL and is representative of FT conditions. Another feature of this station is the sea of clouds present in most of the days at the inversion base (see Fig. 1). The formation of this sea of clouds results mainly of: the forced ascend of the winds arriving to the north face of the island, and the convection by solar heating.

This scenario gives place to a given vertical distribution of gases and aerosols in the station surroundings. The above mentioned temperature inversion defines a discontinuity in the vertical distribution of gases such as H_2O and O_3. In particular, humid MBL air masses carried out until the station by the diurnal mountain breeze, result in typical H_2O increases of 60 % at the level of the station. On the contrary, O_3 suffers

AMTD
6, 8235–8267, 2013

a decrease of 6.5 % (Cuevas et al., 1992; Puentedura et al., 2012). These variations in concentration can be used as signatures of the origin of the air masses over the station. Concerning the aerosols content, two typical situations can be found at Izaña: very clean days with Aerosol Optical Depth (AOD) below 0.05, or dusty days with AOD ranging between 0.2 and 0.8, due to Saharan dust transported from North Africa.

1.2 Modified Geometrical Approach (MGA)

MAX-DOAS is an extension of DOAS technique in which SCD of absorbers can be obtained from solar scattered radiation collected at multiple viewing directions. SCD is defined as the gas density (c) integrated along the effective light path (s). The effective light path is actually the average of an infinite number of different light paths, weighted by the radiation intensity reaching the instrument. In other words, it is the most probable path followed by light under given conditions:

$$\mathrm{SCD} = \int c(s)ds \tag{1}$$

In the proposed MGA the SCDs of the gas of interest for two instrument elevation angles (IEA): $\alpha = 0^\circ$ and $\alpha = 90^\circ$ are considered. Also it is assumed that for both geometries the scattering altitude is the same and is close to the station level. Under these assumptions, the horizontal path (d) is the difference between the optical paths of both situations (see Fig. 2). Then, for a homogeneous layer, the concentration of the gas at the level of the station (c_{St}), can be estimated as follows:

$$c_{\mathrm{St}} = \frac{\mathrm{SCD}(\alpha = 0^\circ, \theta_1, t_1) - \mathrm{SCD}(\alpha = 90^\circ, \theta_2, t_2) f}{d}, \tag{2}$$

where θ_i is the SZA of the measurements at time t_i, and $f = \cos(\theta_2)/\cos(\theta_1)$ is a correction factor accounting for the difference in SZA between horizontal (IEA = 0°) and zenith (IEA = 90°) measurements.

AMTD
6, 8235–8267, 2013

Within the MGA, two different methods have been considered to estimate d: O_4-MGA and AMF-MGA. The first one uses SCD of O_4 (SCD_{O_4}) measured simultaneously to the gases which concentration is to be retrieved. O_4-MGA also uses mean O_4 density (c_{O_4}) of the layer between the station altitude (h_s) and the effective scattering altitude (h) (see Fig. 2). O_4 density at a given altitude can be easily estimated from oxygen density, whose vertical distribution in the atmosphere is proportional to air density. This first procedure has the advantage that no radiative transfer models are needed.

$$d = \frac{\mathrm{SCD}_{O_4}(\alpha = 0^\circ, \theta_1, t_1) - \mathrm{SCD}_{O_4}(\alpha = 90^\circ, \theta_2, t_2) f}{c_{O_4}}, \quad (3)$$

In the second method (AMF-MGA), the AMF of the considered gas is used to obtain f and d. AMF gives the ratio between the SCD and the VCD, being VCD the gas concentration integrated over the vertical path (z) along the atmosphere:

$$\mathrm{VCD} = \int c(z) dz, \quad (4)$$

AMF depends on the wavelength (λ), the SZA (θ), the IEA (α), and the relative azimuth angle (ϕ) between the sun and the instrument. Assuming a single scattering atmosphere and neglecting the refraction, AMF can be written as:

$$\mathrm{AMF}(\alpha, \theta, \phi, \lambda) = \frac{\mathrm{SCD}(\alpha, \theta, \phi, \lambda)}{\mathrm{VCD}} = \frac{s}{H}, \quad (5)$$

where H is the height between the scattering altitude and the top of the atmosphere, and s is the optical path followed by the solar beams until the scattering altitude. The correction factor (f') within the AMF-MGA is then given by:

$$f' = \frac{s(\alpha = 90^\circ, \theta_1, t_1)}{s(\alpha = 90^\circ, \theta_2, t_2)} = \frac{\mathrm{AMF}(\alpha = 90^\circ, \theta_1, t_1)}{\mathrm{AMF}(\alpha = 90^\circ, \theta_2, t_2)}, \quad (6)$$

AMTD
6, 8235–8267, 2013

and the horizontal paths for each geometry (d') are obtained from the radiative transfer model (at θ_1). Then, the gas concentration can be estimated similarly as in Eq. (2):

$$c_{St} = \frac{SCD(\alpha = 0^\circ, \theta_1, t_1) - SCD(\alpha = 90^\circ, \theta_2, t_2) f'}{d'}. \quad (7)$$

For the calculation of d' with the radiative transfer model, n layers (1 km wide in this calculation) of constant concentration and width are considered, from the top of the atmosphere to the station level (See Fig. 3). If the optical path of each layer before and after the scattering is named as Δs_b and Δs_a respectively, and we consider that the scattering happens in the layer where the instrument is placed (layer n), we can write (Beer–Lambert law):

$$\Delta s_b (c_1 + c_2 + \ldots + c_{n-1}) = \frac{1}{\sigma} \ln \left(\frac{I_0}{I} \right)_{n-1}, \quad (8)$$

where c_i is the concentration of the layer i, and σ is the cross section of the given gas and wavelength. I and I_0 are the radiations arriving until the layer $n-1$, with and without consider gas absorption of the gas respectively. Similarly, for the layer where the scattering takes place:

$$\Delta s_a c_n = \frac{1}{\sigma} \ln \left(\frac{I_0}{I} \right)_n - \Delta s_b (c_1 + \ldots + c_n) = \frac{1}{\sigma} \left[\ln \left(\frac{I_0}{I} \right)_n - \ln \left(\frac{I_0}{I} \right)_{n-1} \right], \quad (9)$$

Radiances can be obtained with the radiative transfer model. Optical paths of each layer before and after scattering can then be easily obtained from Eqs. (8) and (9). The total optical path, s, is then calculated as:

$$s = (n-1)\Delta s_b + \Delta s_a, \quad (10)$$

The difference between the total optical path for IEA 0° and 90° gives d'.

AMTD
6, 8235–8267, 2013

1.3 MAX-DOAS measurements and data

MAX-DOAS measurements were performed at a terrace on Izaña station using INTA spectrometer RASAS-II, in summer 2011. In Table 1 we summarise all of the instrument settings, for further details we refer to Roscoe et al. (2010) and Puentedura et al. (2012). Note that the field of view of the light collector was narrowed (with respect to previous works) to 1°, thus reducing the uncertainties on the scanned air masses. Most of the instrument collected radiation comes from the FT (Puentedura et al., 2012), with the largest contribution coming from the station level. RASAS-II is pointing toward North and collects scattered radiation from several elevation angles ranging between −1° and 90°. However, since during subtropical summer at noon the sun is directly overhead, to avoid direct sun on the detector the zenith data was not collected. Data at IEA = 70° has been used instead in our calculations. Consequently, SCD_y in Eqs. (3) and (7) corresponds to $\alpha = 70°$, instead of 90°. The impact of this change was tested and found to be negligible.

Spectra recorded by RASAS-II were processed to obtain the SCDs of O_3, O_4 and NO_2. This retrieval was performed using a code developed at INTA (Gil et al., 2008) that is based on the standard DOAS technique (Platt and Stutz, 2008). The studied wavelengths, ranging from 430 to 500 nm, differ from those suggested by the Network for the Detection of Atmospheric Composition Change (NDACC) in order to avoid the strong H_2O absorption band at 500–510 nm. The retrieved SCDs of O_3 and NO_2 have molecular errors of (2–6) × 10^{17} molec cm^{-2} and (1–3) × 10^{14} molec cm^{-2}, respectively, being the largest at low IEA = 0°. These errors represent 15–20 % of the typical differential SCD (DSCD). In the case of the O_4, the molecular error of DSCD is bellow 1 % under clear sky conditions. A standard diurnal evolution of DSCDs of O_3, NO_2, O_4 and H_2O on a clear day for all IEA is shown in Fig. 4. Note that NO_2 and O_3 DSCD plots have a marked u-shape due to their high concentration at the stratosphere. On the other hand, this signature is not present on the DSCDs of O_4 since its concentration on the stratosphere is negligible.

AMTD
6, 8235–8267, 2013

1.4 In situ measurements

The performance of O_4-MGA and AMF-MGA was tested by comparing their estimated concentrations of O_3 and NO_2 with the in situ measurements available at Izaña observatory. NO_2 and O_3 in situ concentrations were respectively measured with a chemiluminiscence NO-NO_2-NO_x analyzer (Model 42C-TL, Thermo Electron Corporation), and two UV photometric O_3 analyzers running in parallel (Model 49C, Thermo Electron Corporation). The sampled air masses were captured by two inlet systems on the top of the observation tower, located 4m above the terrace. One of the inlets is used for O_3 determination, while the second is used for measuring the rest of the trace gases. Furthermore a laminar vertical flux manifolds ensure residence times of the air masses along the sampling to be smaller than 10 s. The quality control for ozone (Cuevas et al., 2003) includes: 15 min daily check of zeros; Calibration of O_3 analyzer with a primary standard model 49C-PS; quality audits periodically performed by the World Calibration Centre (WCC-EMPA). The calibration of the NO_2 analyzer (Gonzalez, 2012) is performed using a multigas calibrator and certified gas bottles provided by Air Liquide s.a. The Environmental Protection Agency of Unites States (EPA) and the European Union have declared these measurement techniques as reference methodologies. Furthermore they fulfil the Global Atmospheric Watch Programme requirements.

The main drawback of measurements provided by these instruments is that they are local and usually affected by the MBE (e.g. Cuevas et al., 1992; Reidmiller et al., 2012). As a result, they are not representative of FT conditions. In addition to the MBE, dominant synoptic wind exists at the level of the station. The stronger the synoptic wind the lesser the influence of the MBE on these in situ measurements (Cuevas et al., 2013).

Ozone sounding data of the NDACC program are also available. Ozonesondes are launched on a weekly basis from the Orotava station (28°25′ N, 16°18′ W), in Puerto de la Cruz (Tenerife), at a horizontal distance of about 13 km from Izaña. Ozone soundings provide O_3 concentration and meteorological data (pressure, temperature and

AMTD
6, 8235–8267, 2013

humidity) from sea level to 30–35 km of altitude, with a vertical resolution of 100–150 m (Cuevas et al., 1994). O_3 is measured by the standard ECC method (Thompson et al., 2011).

2 Results and discussion

In order to prove that the scattering altitude for elevation angles 0° and 90° is similar, one of the assumptions of the approximation presented in this work, we have used SDISORT (Dahlback and Stamnes, 1991) to calculate single scattering O_3 differential box-AMFs (respect to the zenith) given by this expression:

$$\text{DiffAMF} = [\text{AMF}(\alpha) - \text{AMF}(90^\circ)]\,\Delta z \tag{11}$$

where α is a given elevation angle, and Δz is the widht of the layers of constant concentration considered in the radiative transfer model (100 m in this case). This magnitude provides the difference of the optical paths for both elevation angles (α and 90°) for each of these layers. The results are shown in Fig. 5. As it can be observed, for elevation angle = 0° , the differential box-AMFs become zero at around 3 km of altitude. Above this altitude, the difference between the optical paths of both elevation angles is zero. We can then conclude that the differences in scattering take place below 3 km of altitude. As the observatory is located at 2.4 km of altitude (approximately), this means that the scattering happens only 0.6 km above the station (as maximum).

O_3 and NO_2 concentrations at Izaña station were then estimated using both O_4-MGA and AMF-MGA. Only measurements taken on clear sky days were considered here. Figure 6 shows AERONET level 2 (cloud screened and calibrated data) AOD at 500 nm obtained by the CIMEL photometer over the station during the month of July and the beginning of August. Five well-identified Saharan events took place during this period. The rest of the days presented clear skies with typical AOD below 0.05. In this period we have selected a set of 9 summer days (days 200–208 of 2011), with the first

AMTD
6, 8235–8267, 2013

8 corresponding to clear sky days. In the last day only the first hours were considered since in the afternoon Saharan dust arrived to the station.

For our O_4-MGA simulations, O_4, O_3 and NO_2 SCDs were simultaneously measured by the MAX-DOAS spectrometer. The other necessary parameter in Eq. (3) is the O_4 density (c_{O_4}), which can be easily obtained from the vertical air distribution. Since variations of pressure at Izaña Observatory are smaller than 2.3 % in summer and 5 % in winter, monthly climatology over the station was used in this work.

Concerning AMF-MGA, AMFs were calculated from the radiances obtained by the pseudo-spherical discrete ordinate solver SDISORT (Dahlback and Stamnes, 1991) included in the software package libradtran (Mayer and Kylling, 2005). Vertical profiles of gas densities were taken from AFGL standard atmosphere for tropical latitudes. Due to the low AOD found in the station for the selected days, no aerosols were considered in the simulations. Furthermore, to reproduce as much as possible the conditions of the site, a homogeneous cloud located between 600 and 1100 m a.s.l. was included in the model. The altitude values of the cloud top and base were estimated from the European Centre for Medium-Range Weather Forecasts (ECMWF), using summer conditions of the years 2008 to 2011 for 24 h forecast computed in intervals of 6 h. These altitude values are in good agreement with radio-soundings, which also demonstrated that they present a small variability during summer (Juan José Bustos, private communication, 2010). Also, we have used an optical depth of the cloud equal to 5 (at 500 nm), as catalogued in the International Satellite Cloud Climatology Project (ISCCP). A standard marine surface albedo of 0.07 has been used. Since no appreciable difference is observed in our results when daily solar azimuth variation is considered, the relative azimuth was set to zero. Calculations were performed at 440 nm for O_3 and NO_2. Under these conditions (summarized in Table 1), values of the difference between de optical path for zenith and horizon views, (d in the equations) have been obtained for SZA from 0° to 85° in steps of 1°. For intermediate values, linear interpolation was used.

AMTD
6, 8235–8267, 2013

2.1 Ozone concentration

In Fig. 7, O_3 mixing ratio obtained using O_4-MGA (grey) and single scattering AMF-MGA (red) are compared to O_3 in situ measurements (black). Note that the approximation is more adapted to single scattering because of the assumed geometry. Concentrations based on O_4-MGA yield similar diurnal evolution than those obtained using AMF-MGA. In Fig. 7 is also noticeable a periodic pattern on the diurnal variability of the MGA concentrations. In particular, in contrast with in-situ measurements, decreasing values toward the evening are obtained with the MGA regardless the method used to calculate the optical path. The inverted U-shape with the maximum around noon seems to be related with an incomplete correction of the variation in the stratospheric AMF. Nevertheless, there is in general a good agreement between MGA methods and the in situ measurements, with the MGA capturing the day-to-day variability. However, MGA values are in general larger than the in situ O_3 concentrations. Bellow we explain some of the possible causes that lead to this discrepancy.

The O_4-MGA method relies on the accuracy of the O_4 absorption cross-sections that are known to have large uncertainties (Wagner et al., 2002). Even at room temperature, O_4 cross sections reported in literature (Greenblatt et al., 1990; Hermans et al., 1999) seem to provide DSCDs that are overestimated up to 30 % (Wagner et al., 2009; Clemer et al., 2010). Over Izaña, the opposite behaviour is found, since smaller O_4 cross sections should be required to shift the O_3 concentrations to the in situ ones.

The difference between the MGA and in-situ measurements might be also related to the different air masses sampled by MAX-DOAS and in situ instruments. While the latter provides local information at the site, the former represents the average value along a path of 60–70 km. Therefore, MAX-DOAS spectrometer is providing the O_3 background in the FT. On the other hand, in-situ observations are affected by the MBE that yields to lower ozone content during light period. As a result of the MBE, the averaged differences between hourly mean surface O_3 and the night background level can be up to −20 ppbv on certain summer days (Cuevas et al., 2013). To test if in situ

AMTD
6, 8235–8267, 2013

concentrations used in this work differ from those of the open background, data from the only ozone-sounding launched during the reported period (on day 208) has been used (Fig. 7). O_3 value from the ozonesonde at Izaña level agrees well with estimated MGA values. Note that at the time the ozone-sounding was launched (12:00 UTC), the AOD was below 0.05, therefore representative of a clean day. It is still worthwhile mentioning that during the considered period of time (days 200–208), the in situ measurements were stopped around noon for technical reasons. As a result MAX-DOAS and in situ measurements overlap only on some daylight hours. This could also be a cause of the observed differences between MGA and in situ O_3 concentrations. To test this hypothesis, in Fig. 8, we plot the mean diurnal O_3 volume mixing ratios for AMF-MGA (black) and in situ (blue) from day 200 to 207. Daily averages for each instrument were calculated from two sets of data: all available data of each day (squares), and data for those periods of the day where simultaneous measurements are available (circles). Results show that if we consider only simultaneous data, differences between MGA and in situ results are of the same order than those obtained using all the available data of each day. Based on this we can safely exclude this in-situ noon blackouts as the cause of the difference between MGA and in situ data. Daily averaged O_3 concentrations of MGA and in situ are in agreement when considering error bars.

2.2 NO_2 concentration

The same procedure used for O_3 has been followed to obtain NO_2 concentrations. To account for photochemical changes, AMFs were calculated using NO_2 profiles obtained either hourly either from a standard atmosphere. This allowed us to test the sensitivity of the retrieved concentration on the profile. The hourly profiles were obtained using a photochemical box model (Denis et al., 2005) derived from SLIMCAT 3-D chemical transport model (Chipperfield, 2006).

In Fig. 9, NO_2 results of AMF-MGA are shown together with the in situ data (black). Results do not show large differences when hourly (red) or single (green) profiles of NO_2 are considered. Nevertheless, concentrations obtained using hourly profiles are

AMTD
6, 8235–8267, 2013

a little higher than those estimated using a single profile. A third data set (in grey) has been computed using O_4-MGA. Using this method, lower values are obtained. At so low NO_2 concentrations, there are no tools available to decide which of the three retrievals is the most accurate. As mentioned previously, in situ NO_2 measurements are shown as a reference since during the night-time the NO_2 concentrations are below the detection limit given by the manufacturer.

Contrary to what was observed for the O_3, in-situ NO_2 measurements have higher concentrations during daytime and lower concentrations at the night-time. This difference is explained by the MBE. This mountain breeze brings to the station anthropogenic NO_2 originated over the populated areas around the coast, and therefore increases the mixing ratios up to hundreds of ppts around noon (Fig. 9). In these conditions, the in situ data are not representative of FT (Volz-Thomas et al., 1993; Puentedura et al, 2012). However, this local effect of no more than few hundreds of meters above the surface is smoothed away in the long paths sampled by MAX-DOAS. At night, a well-developed catabatic regime assures that measured NO_2 is representative of FT conditions.

NO_2 concentrations obtained from MGA, presented in this work, were also compared with previous FT NO_2 measurements obtained from research aircraft flights. Bucsela et al. (2008) measured NO_2 over the eastern Atlantic coast of North America during the Intercontinental Chemical Transport Experiment – North America, Phase A (INTEX-A), and the International-Consortium-for-Atmospheric-Research-and-Transformation (ICARTT) aircraft campaigns using the research DC-8 of NASA. These measurements were obtained using the UC Berkeley Laser Induced Fluorescence instrument (TD-LIF), whose detection limit is 4 ppt. These profiles show NO_2 concentration values that are similar to those found in this work (around 20 ppt) for the same altitude and the same period of the year (Martin et al., 2006; Bucsela et al., 2008).

AMTD
6, 8235–8267, 2013

3 Summary and conclusions

A new method, MGA, was developed to obtain surface mixing ratios of trace gases in the FT. MGA uses horizontal and near-zenith geometries to estimate the station level differential path. Two independent methods were used for optical path calculation: the first one, O_4-MGA, uses MAX-DOAS SCDs of O_4, while the second, AMF-MGA, obtains optical paths from AMFs calculated using RTM.

Both methods, O_4-MGA and AMF-MGA, were applied to MAX-DOAS measurements at Izaña observatory in order to estimate FT O_3 and NO_2 mixing ratios. Comparing these results with in-situ measurements we showed that under low aerosol loading, the mixing ratios of O_3 and NO_2 can be retrieved with low errors. The daily averaged MGA O_3 concentrations are in agreement, within the error bars, with the O_3 in situ measurements. Day to day O_3 variations are also well captured by MGA. NO_2 concentrations obtained with MGA are within the range of 20–40 ppt, thus below the detection limit of the in situ chemiluminiscent analyzer. Nevertheless they are in good agreement with other subtropical free troposphere measurements carried out from aircraft (Martin et al., 2006; Bucsela et al., 2008).

The main advantage of the MGA methods is that they provide mixing ratios that are barely affected by MBE. Since air masses sampled by MAX-DOAS spectrometer extend few tens of kms, inhomogeneities are smoothed along the path. Therefore, unlike in situ data, MAX-DOAS measurements are representative of the FT. Furthermore, MGA methods provide a simple way to estimate O_3 mixing ratios when no in situ instruments are available. In fact, for NO_2 it constitutes the only way to monitor concentrations of few tens of ppt, which are below the detection limits of the standard instrumentation based on chemiluminiscence.

Acknowledgements. Laura Gomez thanks the MINECO (Spanish Economy Ministry) for funding *Juan de la Cierva* grant. We acknowledge the support of AMISOC (Atmospheric Minor Species relevant to the Ozone Chemistry at both sides of the Subtropical jet, contract number CGL2011-24891), and NORS (Demonstration Network Of ground-based Remote Sensing Observations in support of the GMES Atmospheric Service) Integrated Project under the 7th

AMTD
6, 8235–8267, 2013

Framework Program (contract number FP7-SPACE-2011-284421). The authors thank Ramón Ramos and the CIAI staff for their support at Izaña Observatory and the Sieltec team for instrument maintenance. We thank Philippe Goloub for his effort in establishing and maintaining AERONET Izaña site.

References

Beelen, R., Hoek, G., Pebesma, E., Vienneaud, D., Hoogh, K., and Briggs, D. J.: Mapping of background air pollution at a fine spatial scale across the European Union, Sci. Total Environ., 407, 1852–1867, doi:10.1016/j.scitotenv.2008.11.048, 2009.

Bogumil, K., Orphal, J., Flaud, J. M., and Burrows, J. P.: Vibrational progressions in the visible and near ultraviolet absorption spectrum of ozone, Chem. Phys. Lett., 349, 241–248, 2001.

Bucsela, E. J., Perring, A. E., Cohen, R. C., Boersma, K. F., Celarier, E. A., Gleason, J. F., Wening, M. O., Bertram, T. H., Wooldridge, P. J., Dirkisen, R., and Veefkind, J. P.: Comparison of tropospheric NO_2 from in situ aircraft measurements with near-real-time and standard product data from OMI, J. Geophys. Res., 113, D16S31, doi:10.1029/2007JD008838, 2008.

Chipperfield, M. P.: New version of the TOMCAT/SLIMCAT off-line chemical transport model: Intercomparison of stratospheric tracer experiments, Q. J. Roy. Meteorol. Soc., 132, 1179–1203, doi:10.1256/qj.05.51, 2006.

Clémer, K., Van Roozendael, M., Fayt, C., Hendrick, F., Hermans, C., Pinardi, G., Spurr, R., Wang, P., and De Mazière, M., Multiple wavelength retrieval of tropospheric aerosol optical properties from MAXDOAS Measurements in Beijing, Atmos. Meas. Tech., 3, 863–878, doi:10.5194/amt-3-863-2010, 2010.

Cuevas, E., Díaz, A., and Martín, F.: Atmospheric Carbon Dioxide Concentration at Izaña BAPMoN Observatory, Canary Islands, 1984-1990, in: Proceedings 19th ITM on Air Pollution Modeling and its Applications, NATO/CCMS, Ierapetra, Greece, 29 September–4 October 1991, 45–46, edited by: van Dop, H. and Kallos, G., Plenum Press, New York, USA, 1992.

Cuevas, E., Lamb, K., and Bais, A.: Total Ozone Contents derived by Different Instruments and Soundings, Meteorological Publications No 27, Finnish Meteorological Institute, 105–119, Helsinki, 1994.

Cuevas, E., González, Y., Rodríguez, S., Guerra, J. C., Gómez-Peláez, A. J., Alonso-Pérez, S., Bustos, J., and Milford, C.: Assessment of atmospheric processes driving ozone varia-

AMTD
6, 8235–8267, 2013

tions in the subtropical North Atlantic free troposphere, Atmos. Chem. Phys., 13, 1973–1998, doi:10.5194/acp-13-1973-2013, 2013.
Dahlback, A. and Stamnes, K.: A new spherical model for computing the radiation field available for photolysis and heating at twilight, Planet. Space Sci., 39, 671–683, doi:10.1016/0032-0633(91)90061-E, 1991.
Denis, L., Roscoe, H. K., Chipperfield, M. P., Van Roozendael, M., and Goutail, F.: A new software suite for NO_2 vertical profile retrieval from ground-based zenith-sky spectrometers, J. Quant. Spectrosc. Ra., 92, 321–333, doi:10.1016/j.jqsrt.2004.07.030, 2005.
Engardt, M., Bergström, R., and Andersson, C.: Climate and Emission Changes Contributing to Changes in Near-surface Ozone in Europe over the Coming Decades: Results from Model Studies, Ambio, 38, 452–458, 2009.
Fayt, C. and Van Roozendael, M.: WinDOAS 2.1. User Manual, IASB-BIRA, 2001.
Font, I.: El Tiempo Atmosférico de las Islas Canarias, Servicio Meteorológico Nacional (INM), Serie A, No. 26, 1956.
Gil, M., Yela, M., Gunn, L. N., Richter, A., Alonso, I., Chipperfield, M. P., Cuevas, E., Iglesias, J., Navarro, M., Puentedura, O., and Rodríguez., S.: NO_2 Climatology in the Northern Subtropical Region: Diurnal, Seasonal and Interannual variability, Atmos. Chem. Phys., 8, 1635–1648, doi:10.5194/acp-8-1635-2008, 2008.
González, Y.: Levels and origin of reactive gases and their relationship with aerosols in the proximity of emission sources and in the free troposphere at Tenerife, PhD Thesis, Universidad de la Laguna (Canary islands, Spain), 2012.
Greenblatt, G. D., Orlando, J. J., Burkholder, J. B., and Ravishankara, A. R.: Absorption Measurements of Oxygen Between 330 and 1140 nm, J. Geophys. Res., 95, 18577–18582, 1990.
Hendrick, F., Pommereau, J. P., Goutail, F., Evans, R. D., Ionov, D., Pazmino, A., Kyrö, E., Held, G., Eriksen, P., Dorokhov, V., Gil, M., and Van Roozendael, M.: NDACC/SAOZ UV-visible total ozone measurements: improved retrieval and comparison with correlative ground-based and satellite observation, Atmos. Chem. Phys., 11, 5975–5995, doi:10.5194/acp-11-5975-2011, 2011.
Hermans, C., Vandaele, A.C., Carleer, M., Fally, S., Colin, R., Jenouvrier, A., Coquart, B., and Mérienne, M. F.: Absorption Cross-Sections of Atmospheric Constituents: NO_2, O_2 and H_2O, Environ. Sci. Poll. Res., 6, 151–158, doi:10.1007/BF02987620, 1999.

AMTD
6, 8235–8267, 2013

Hintsa, E. J., Allsup, G. P., Eck, C. F., Hosom, D. S., Purcell, M. J., Roberts, A. A., Scott, D. R., Sholkovitz, E. R., Rawlins, W. T., Mulhall, P. A., Lightener, K., McMillan, W. W., Song, J., and Newchurch, M. J.: New Ozone Measurement Systems for Autonomous Operation on Ocean Buoys and Towers, J. Atmos. Ocean. Technol., 21, 1007–1016, doi:10.1175/1520-0426(2004)021$<$1007:NOMSFA$>$2.0.CO;2, 2004.

Hönninger, G. and Platt, U.: Observations of BrO and its vertical distribution during surface ozone depletion at Alert, Atmos. Environ., 36, 2481–2489, doi:10.1016/S1352-2310(02)00104-8, 2002.

Hönninger, G., von Friedeburg, C., and Platt, U.: Multi axis differential absorption spectroscopy (MAX-DOAS), Atmos. Chem. Phys., 4, 231–254, doi:10.5194/acp-4-231-2004, 2004.

Ionov, D. V. and Timofeev, Y. M.: Regional Space Monitoring of Nitrogen Dioxide in the Troposphere, Atmos. Ocean. Phys., 45, 434–443, doi:10.1134/S0001433809040045, 2009.

Liang, O., Jaeglé, L., Jaffe, D. A., Weiss-Penzias, P., Heckman, A., and Snow, J. A.: Long-range transport of Asian pollution to the northeast Pacific: Seasonal variations and transport pathways of carbon monoxide, J. Geophys. Res., 109, D23S07, doi:10.1029/2003JD004402, 2004.

Mao, H., Talbot, R., Troop, D., Johnson, R., Businger, S., and Thompson, A. M.: Smart balloon observations over the North Atlantic: O_3 data analysis and modelling, J. Geophys. Res., 111, D23S56, doi:10.1029/2005JD006507, 2006.

Martin, R. V., Sioris, C. E., Chance, K., Ryerson, T. B., Bertram, T. H., Wooldridge, P. J., Cohen, R. C., Neuman, J. A., Swanson, A., and Flocke, F. M.: Evaluation of space-based constraints on global nitrogen oxide emissions with regional aircraft measurements over and downwind of eastern North America, J. Geophys. Res., 111, 5308, doi:10.1029/2005JD006680, 2006.

Martin, M., Pöhler, D., Seitz, K., Sinreich, R., and Platt, U.: BrO measurements over the Eastern North-Atlantic, Atmos. Chem. Phys., 9, 9545–9554, doi:10.5194/acp-9-9545-2009, 2009.

Mayer, B. and Kylling, A.: Technical note: The libRadtran software package for radiative transfer calculations – description and examples of use, Atmos. Chem. Phys., 5, 1855–1877, doi:10.5194/acp-5-1855-2005, 2005.

Milford, C., Marrero, C., Martin, C., Bustos, J. J., and Querol, X.: Forecasting the air pollution episode potential in the Canary Islands, Adv. Sci. Res., 2, 21–26, doi:10.5194/asr-2-21-2008, 2008.

Oltmans, S. J., Levy, H., Harris, J. M., Merrill, J. T., Moody, J. L., Lathrop, J. A., Cuevas, E., Trainer, M., O'Neill, M. S., Prospero, J. M., Vömel, H., and Jonson, B. J.: Summer and spring

AMTD
6, 8235–8267, 2013

ozone profiles over the North Atlantic from ozonesonde measurements, J. Geophys. Res., 101, 29179–29200, doi:10.1029/96JD01713, 1996.
Platt, U. and Stutz, J.: Differential Optical Absorption Spectroscopy: Principles and Applications, Springer-Verlag, Berlin, Germany, 2008.
Puentedura, O., Gil, M., Saiz-Lopez, A., Hay, T., Navarro-Comas, M., Gómez-Pelaez, A., Cuevas, E., Iglesias, J., and Gomez, L: Iodine Monoxide in the North Subtropical free Troposphere, Atmos. Chem. Phys., 12, 4909–4924, doi:10.5194/acp-12-4909-2012, 2012.
Reidmiller, D. R., Jaffe, D. A., Fischer, E. V., and Finley, B.: Nitrogen oxides in the boundary layer and free troposphere at the Mt. Bachelor Observatory, Atmos. Chem. Phys., 10, 6043–6062, doi:10.5194/acp-10-6043-2010, 2010.
Robinson, A. D., Millard, G. A., Danis, F., Guirlet, M., Harris, N. R. P., Lee, A. M., McIntyre, J. D., Pyle, J. A., Arvelius, J., Dagnesjo, S., Kirkwood, S., Nilsson, H., Toohey, D. W., Deshler, T., Goutail, F. , Pommereau, J. P., Elkins, J. W., Moore, F., Ray, E., Schmidt, U., Engel, A., and Müller, M.: Ozone loss derived from balloon-borne tracer measurements in the1999/2000 Arctic winter, Atmos. Chem. Phys., 5, 1423–1436, doi:10.5194/acp-5-1423-2005, 2005.
Rodgers, C. D.: Inverse Methods for Atmospheric Sounding: Theory and Practice, Vol. 2 of Atmospheric, Oceanic and Planetary Physics, World Scientific, Hackensack, NJ, doi:10.1142/9789812813718, 2000.
Roscoe, H. K., VanRoozendael, M., Fayt, C., du Piesanie, A., Abuhassan, N., Adams, C., Akrami, M., Cede, A., Chong, J., Clémer, K., Friess, U., Gil Ojeda, M., Goutail, F., Graves, R., Griesfeller, A., Grossmann, K., Hemerijckx, G., Hendrick, F., Herman, J., Hermans, C., Irie, H., Johnston, P. V., Kanaya, Y., Kreher, K., Leigh, R., Merlaud, A., Mount, G. H., Navarro, M., Oetjen, H., Pazmino, A., Perez-Camacho, M., Peters, E., Pinardi, G., Puentedura, O., Richter, A., Schönhardt, A., Shaiganfar, R., Spinei, E., Strong, K., Takashima, H., Vlemmix, T., Vrekoussis, M., Wagner, T., Wittrock, F., Yela, M., Yilmaz, S., Boersma, F., Hains, J., Kroon, M., and Piters, A.: Intercomparison of slant column measurements of NO_2 and O_4 by MAX-DOAS and zenith-sky UV and visible spectrometers, Atmos. Meas. Tech. Discuss., 3, 3383–3423, doi:10.5194/amtd-3-3383-2010, 2010.
Rothman, L. S., Gordon, I. E., Barbe, A., Benner, D. C., Bernath, P. F., Birk, M., Boudon, V., Brown, L. R., Campargue, A., Champion, J. P., Chance, K., Coudert, L. H., Danaj, V., Devi, V. M., Fally, S., Flaud, J. M., Gamache, R. R., Goldmanm, A., Jacquemart, D., Kleiner, I., Lacome, N., Lafferty, W. J., Mandin, J. Y., Massie, S. T., Mikhailenko, S. N., Miller, C. E., Moazzen-Ahmadi, N., Naumenko, O. V., Nikitin, A. V., Orphal, J., Perevalov, V. I., Perrin,

AMTD
6, 8235–8267, 2013

A., Predoi-Cross, A., Rinsland, C. P., Rotger, M., Simecková, M., H.Smith, M. A., Sung, K., Tashkun, S. A., Tennyson, J., Toth, R. A., Vandaele, A. C., and VanderAuwera., J.: The HITRAN 2008 molecular spectroscopic database, J. Quant. Spectrosc. Ra., 110, 533–572, doi:10.1016/j.jqsrt.2009.02.013, 2009.

Sinreich, R., Merten, A., Molina, L., and Volkamer, R.: Parameterizing radiative transfer to convert MAX-DOAS dSCDs into near-surface box averaged mixing ratios and vertical profiles, Atmos. Meas. Tech. Discuss., 5, 7641–7673, doi:10.5194/amtd-5-7641-2012, 2012.

Steck, T.: Methods for determining regularization for atmospheric retrieval problems, App. Optics, 41, 1788–1797, doi:10.1364/AO.41.001788, 2002.

Stohl, A. and Trickl, T.: A textbook example of long-range transport: Simultaneous observation of ozone maxima of stratospheric and North American origin in the free troposphere over Europe, J. Geophys. Res., 104, 30445–30462, doi:10.1029/1999JD900803, 1999.

Stohl, A., Huntrieser, H., Richter, A., Beirle, S., Cooper, O. R., Eckhardt, S., Forster, C., James, P., Spichtinger, N., Wenig, M., Wagner, T., Burrows, J. P., and Platt, U.: Rapid intercontinental air pollution transport associated with a meteorological bomb, Atmos. Chem. Phys., 3, 969–985, doi:10.5194/acpd-3-2101-2003, 2003.

Thakur, A. N., Sing, H. B., Mariani, P., Chen, Y., Wang, Y., Jacob, D. J., Brasseur, G., Müller, J. F., and Lawrence M.: Distribution of reactive nitrogen species in the remote free troposphere: data and model comparison, Atmos. Environ., 33, 1403–1422, doi:10.1016/S1352-2310(98)00281-7, 1999.

Thompson, A. M., Oltmans, S. J., Tarasick, D. W., von der Gathen, P., Smit, H. G. J., and Witte, J. C.: Strategic ozone sounding networks: Review of design and accomplishments, Atmos. Environ., 45, 2145–2163, doi:10.1016/j.atmosenv.2010.05.002, 2011.

Vandaele, A. C., Hermans, C., Simon, P. C., Carleer, M., Colins, R., Fally, S., Mérienne, M. F., Jenouvrier, A., and Coquart, B.: Measurements of the NO_2 Absorption Cross-Sections from 42000 cm−1 to 10000 cm−1 (238–1000 nm) at 220 K and 294 K, J. Quant. Spectrosc. Ra., 59, 171–184, doi:10.1016/S0022-4073(97)00168-4, 1998.

Volz-Thomas, A., Schmitt, R., Cuevas, E., Prospero, J. M., Savoie, D., Graustein, W., and Turekian, K.: Concurrent Measurements of Carbon Monoxide, Ozone, NOy, PAN and Aerosols at Izaña, Tenerife, Atmospheric Chemistry of the North Atlantic and AEROCE II. A31g. 1993 Fall Meeting, American Geophysical Union, p. 145, 1993

Wagner, T., von Friedeburg, C., Wening, M., Otten, C., and Platt, U.: UV-Visible observations of atmospheric O4 absorptions using direct moonlight and zenith-scattered sunlight for clear-

AMTD
6, 8235–8267, 2013

sky and cloudy sky conditions, J. Geophys. Res., 107, 4424, doi:10.1029/2001JD001026, 2002.

Wagner, T., Ibrahim, O., Shaiganfar, R., and Platt, U.: Mobile MAX-DOAS observations of tropospheric trace gases, Atmos. Meas. Tech., 3, 129–140, doi:10.5194/amt-3-129-2010, 2010.

Wenig, M., Spichtinger, N., Stohl, A., Held, G., Beirle, S., Wagner, T., Jähne, B., and Platt, U.: Intercontinental transport of nitrogen oxide pollution plumes, Atmos. Chem. Phys., 3, 387–393, doi:10.5194/acp-3-387-2003, 2003.

Zyryanov, D., Foret, G., Eremenko, M., Beekmann, M., Cammas, J. P., D'Isidoro, M., Elbern, H., Flemming, J., Friese, E., Kioutsioutkis, I., Maurizi, A., Melas, D., Meleux, F., Menut, L., Moinat, P., Peuch, V. H., Poupkou, A., Razinger, M., Schultz, M., Stein, O., Suttie, A. M., Valdebenito, A., Zerefos, C., Dufour, G., Bergametti, G., and Flaud, J. M.: 3-D evaluation of tropospheric ozone simulations by an ensemble of regional Chemistry Transport Model, Atmos. Chem. Phys., 12, 3219–3240, doi:10.5194/acp-12-3219-2012, 2012.

AMTD

6, 8235–8267, 2013

Table 1. Instrumental characteristics and parameters used in the fit of the spectra.

Instrumental		
FWHM		0.52–0.58 nm
Linear dispersion		0.11 nm pixel^{-1}
F.O.V.		1°
Instrument Elevation Angles (IEA)		90°, 70°, 30°, 10°, 5°, 3°, 2°, 1°, 0°, −1°
Azimuth		Fixed to North
Time for collecting a single spectrum		From 0.2s at noon to 10 s at 90°SZA
Time for a single measurement		Spectra co-added for 120 s
Time of a complete cycle		4 min
Fit parameters		
Spectral interval		430–500 nm
Orthogonalization Polynomial		3rd degree
Offset		Inverse of the reference
Reference spectrum		A single one for all period. At zenith and SZA = 70°
Absorption Cross-sections		
Molecule	Temperature	Reference
O_3 ($I_0 = 10^{19}$ molec cm^{-2})	223 K	Bogumil et al. (2001)
NO_2 ($I_0 = 5 \times 10^{16}$ molec cm^{-2})	220 K	Vandaele et al. (1998)
H_2O	296 K	HITRAN update 2009 (Rothman et al., 2008)
O_4	298 K	Hermans et al. (1999)*
Rot. Raman Scatt. (Ring effect)		WINDOAS package (Fayt and Van Roozendael, 2001)

* Data can be found in: http://spectrolab.aeronomie.be/o2.htm.

AMTD
6, 8235–8267, 2013

Table 2. Input parameters used in libradtran for the optical paths calculation.

Libradtran Inputs	
Atmosphere model	Standard Atmosphere for Tropical Latitudes: afglt
Aerosols	No aerosols
Cloud	Optical depth 5, 0.6–1.1 km
Albedo	0.07
Instrument Azimuth	Fixed to North
Solar Azimuth	Fixed to South
Solar zenith angle	From 0°to 85°in steps of 1°
Elevation angle	0.1°and 70°
Wave length	440 nm ($O_3$and NO_2)
Scattering	Single
Cross section (O_3)	Bogumil et al. (2001) (223 K)
Cross section (NO_2)	Vandaele et al. (1998) (220 K)
Solver	SDISORT

AMTD
6, 8235–8267, 2013

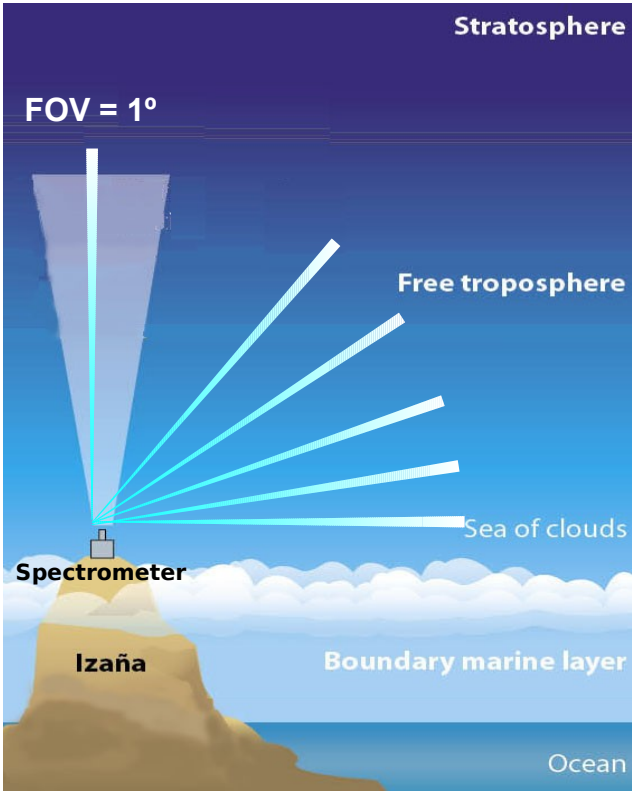

Fig. 1. Scheme of the Izaña station.

AMTD
6, 8235–8267, 2013

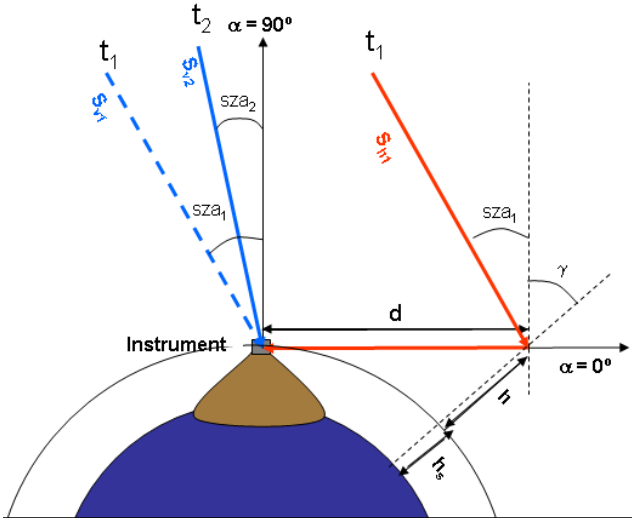

Fig. 2. Schematic representation of a simplified optical path of solar radiation for zenithal (blue) and horizontal (red) observational geometries. See text for explanation.

AMTD
6, 8235–8267, 2013

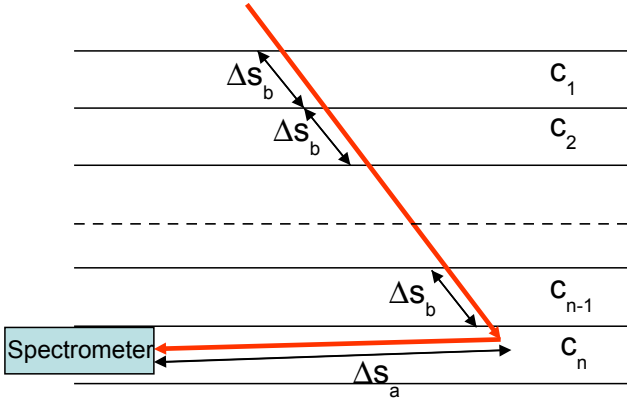

Fig. 3. Schematic representation of assumed layers model and optical path of solar radiation for optical path calculation when using AFM-MGA method. Layers have constant concentration and width.

AMTD
6, 8235–8267, 2013

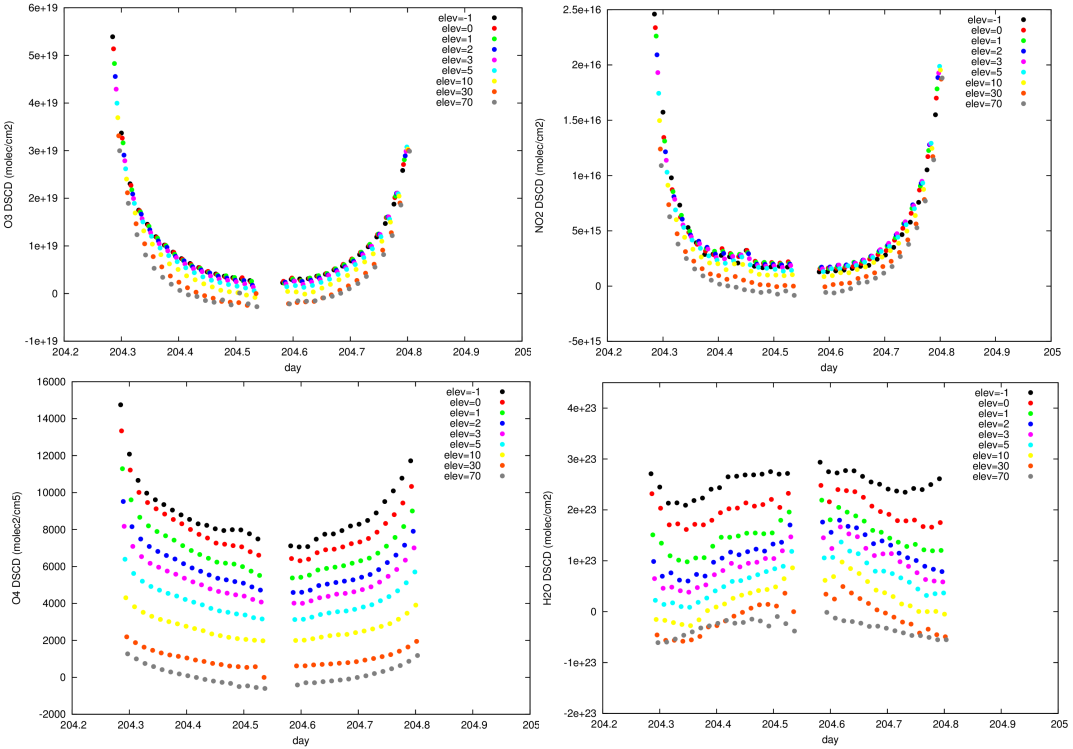

Fig. 4. MAX-DOAS measured DSCD of O_3 (top left), NO_2 (top right) O_4 (bottom left) and H_2O (bottom right) for day 204 and for all elevation angles.

AMTD
6, 8235–8267, 2013

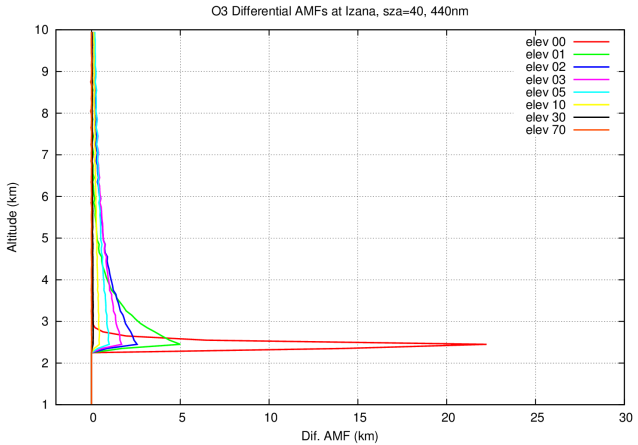

Fig. 5. Differential Box-AMFs (respect to the zenith) for Izaña Observatory. Calculations have been performed at 440 nm.

AMTD
6, 8235–8267, 2013

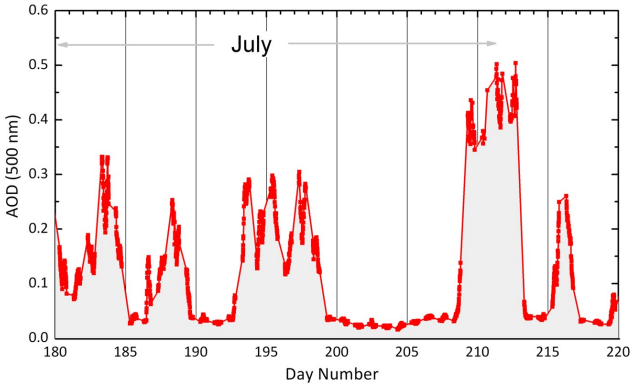

Fig. 6. Integrated AOD at 500 nm, obtained at Izaña station on days 180 to 220 of 2011.

AMTD
6, 8235–8267, 2013

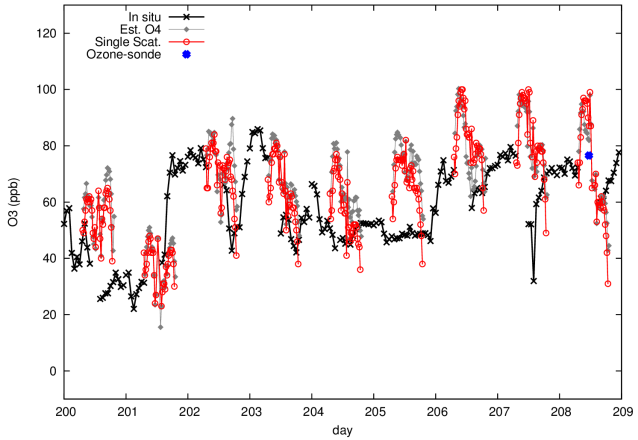

Fig. 7. Surface O_3 mixing ratios (in ppbv) at Izaña Observatory. Red open circles correspond to ozone mixing ratios obtained using single scattering AMF-MGA. Grey diamonds correspond to O_3 mixing ratios obtained using O_4-MGA. Black crosses correspond to in situ measurements. Blue point corresponds to O_3 concentration for the altitude of the station obtained from ozone-sounding.

AMTD
6, 8235–8267, 2013

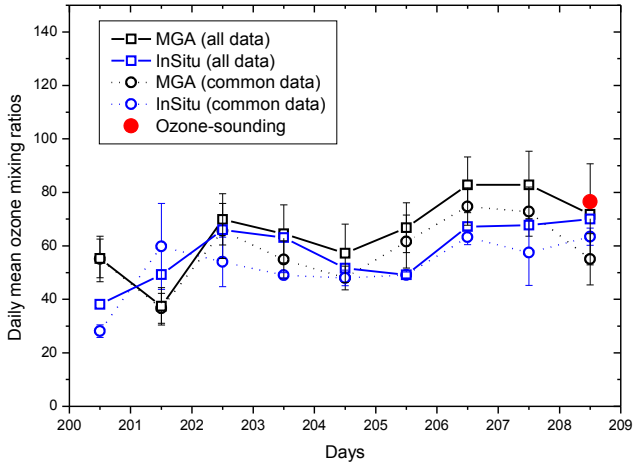

Fig. 8. Daily average values of MGA (black) and in situ (blue) O_3 mixing ratios when using all available data (squares) for each day or data simultaneously recorded (circles) by both instruments. Error bars correspond to standard deviation of MAX-DOAS measurements.

AMTD
6, 8235–8267, 2013

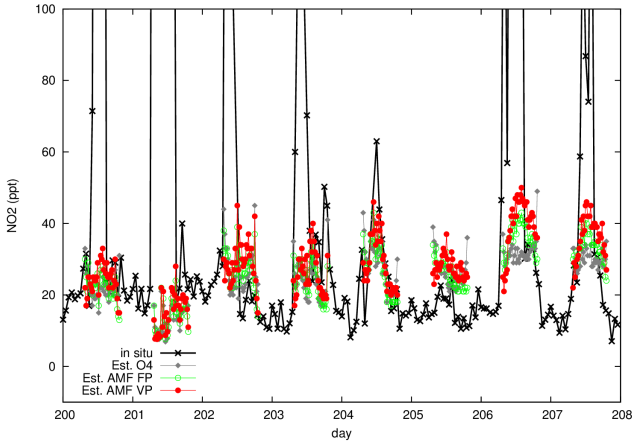

Fig. 9. Surface NO_2 mixing ratios at Izaña Observatory for days 200 to 207. Black crosses correspond to in situ measurements. Grey diamonds correspond to NO_2 mixing ratios obtained with O_4-MGA. Red solid circles and green open circles correspond to NO_2 mixing ratios obtained with AMF-MGA, considering hourly and single profile of NO_2, respectively.

AMTD
6, 8235–8267, 2013